Two-stage Semi-automatic Organ Segmentation Framework using Radial Basis Functions and Level Sets

Andreas Wimmer[1,2], Grzegorz Soza[2], and Joachim Hornegger[1]

[1] Institute of Pattern Recognition, University of Erlangen-Nuremberg, Erlangen, Germany
andreas.wimmer@informatik.uni-erlangen.de
[2] Siemens Medical Solutions, Forchheim, Germany

Abstract. The automatic segmentation of complex anatomical structures often fails due to low-contrast or missing edges, pathologic alterations, or high noise. As an alternative, we propose a novel two-stage semi-automatic algorithm that is able to segment complex structures like the liver shape with moderate user interaction. The first stage of our algorithm is the manual delineation of cross-sections of the anatomical structure in 2-D multi-planar reconstruction views. From this set of contours, an initial 3-D surface is reconstructed using radial basis functions. In a second step, the surface is evolved using a level set algorithm incorporating a new combination of both image information and shape information, the latter being derived from the initial contours. The algorithm has been evaluated for 10 Computed Tomography scans of the liver and has shown promising results.

1 Introduction

The automatic segmentation of complex anatomical structures is still a challenging task. Algorithms relying solely on image intensities or features derived thereof often fail in case of low-contrast or missing edges, as shown in Fig. 1(b). In addition, pathologic structures and high noise, for example due to reduced radiation dose in Computed Tomography (CT), can introduce false edges and irregular feature statistics, hindering edge- or region-based approaches, respectively. In order to cope with missing or ambiguous low-level information, high-level information has been successfully employed, for example in the form of shape priors [1]. This, however, requires modeling anatomical characteristics and demands for a training phase. Considering complex structures with high variations, for example the shape of the liver, it may be difficult or even impossible to capture the set of admissible instances, as illustrated in Fig. 1(a) and 1(c).

A segmentation algorithm incorporating shape information is presented in [2] as part of a framework for the automatic anatomical, pathological, and functional segmentation of the liver in CT scans. The anatomical segmentation involves aligning a liver template followed by the deformation of a shape constrained deformable model using global and local forces.

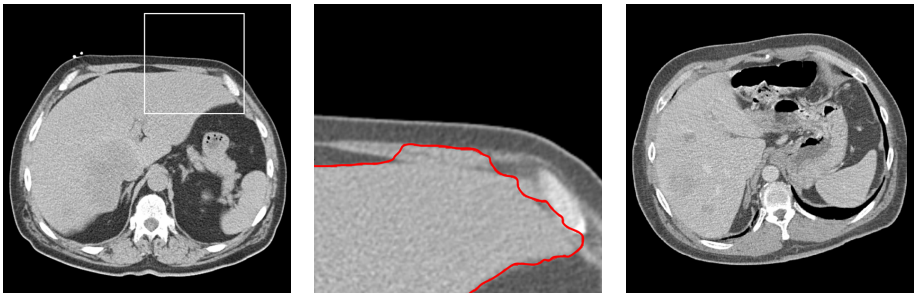

(a) (b) (c)

Fig. 1. (a) Sample CT slice with low-contrast boundary between liver and muscle tissue. (b) Enlarged view of the region marked in (a), segmentation obtained for edge-based Geodesic Active Contours [7] expanding from within the liver. (c) Slice containing the largest extent of another liver, illustrating the high variation in liver shape.

Shape information is also employed in [3], where an Active Shape Model (ASM) approach for the fully automated 3-D segmentation of the liver in CT scans is evaluated for a large number of datasets and different gray-level appearance models guiding the deformation. In order to cope with the huge variety of liver shapes, restrictions of the classical ASM are loosened by incorporating a spring-model deformable mesh.

In [4], a semi-automatic segmentation method for 3-D objects in medical images is presented. The proposed method consists in manually delineating several cross-sections of the anatomical structure in parallel slices using the live wire method [5]. For intermediate slices, contours are determined by shape-based interpolation of contours in slices above and below.

The Random Walker algorithm [6] is a popular semi-automatic segmentation method. The user places labels for each class to be segmented in the volume (or image) in a fashion similar to a painting application. The class of each unlabeled voxel is then determined as the class which has the highest probability of being reached by a random walker starting at the respective position. The probability for the random walker moving from one voxel to another is based on the intensity difference between both voxels.

The lack of knowledge about the location and orientation of the structure, for example due to diseases or different acquisition procedures, poses another major challenge for any segmentation algorithm. Starting from a deficient position, most algorithms will either fail completely, stop at a poor local minimum of their target function, or at best require a large computational effort.

In order to address these problems of varying shape, position, and orientation, we propose a novel two-stage semi-automatic algorithm. Our algorithm starts with the manual delineation of cross-sections of the anatomical structure in 2-D multi-planar reconstruction (MPR) views. This is advantageous compared to the delineation in parallel slices as in [4], where problems arise when the organ surface is almost coplanar to the slice. From this set of contours, an initial 3-D surface is

reconstructed using radial basis functions (RBFs). According to our experience, seven manually drawn contours already are sufficient in order to obtain a good approximation of the complex shape of a liver. In a second stage, this surface is evolved using a level set [8] algorithm incorporating a new combination of both image information and shape information. The shape information is derived from the initial contours and thus tailored to the specific dataset. The inclusion of image information frees the user from having to perform numerous manual delineations. Our paradigm is to specify shape information where image content is ambiguous. In other regions, image information prevails. The algorithm is summarized as follows:

1. Manually delineate cross-sections of the anatomical structure in 2-D MPR views
2. Reconstruct the 3-D surface defined by the manual delineations through radial basis functions
3. Evolve the reconstructed surface under both image and shape information using the level set framework

In Sect. 2, the manual delineation of the anatomical structure and the reconstruction of the initial 3-D surface are presented. Section 3 details the subsequent surface evolution using both image and shape information. Results for the segmentation of the liver shape in CT scans are presented in Sect. 4, followed by a discussion in Sect. 5.

2 Manual Delineation and Surface Reconstruction

The first step in our semi-automatic segmentation algorithm is the manual delineation of cross-sections of the anatomical structure in 2-D MPR views. We have chosen to fit a 2-D cubic interpolating spline [9] through control points placed by the user. Smooth organ shapes usually require the placement of only a couple of control points to capture the cross-section, as can be seen in Fig. 2(a). The user can insert, move, and delete control points. At any time, the current spline curve is shown to the user, providing immediate visual feedback about changes. The contours are defined in three orthogonal views. Complex structures like the liver shape typically require the definition of six to eight contours in total. In Fig. 2(b), six contours are defined, two for each view direction.

Other approaches like the live wire method [5] could easily be integrated into our algorithm, too. Compared to the Random Walker algorithm [6], the definition of accurate spline curves may seem inconvenient and costly. However, as noted above, smooth organ shapes usually require the placement of only a few spline control points, and for low contrast boundaries, the Random Walker may require an exact placement of labels, too.

After the contours have been defined, radial basis functions are used to interpolate an initial surface. It has been demonstrated in [10, 11] that radial basis functions deliver high quality smooth surface reconstructions even for sparse datasets. The surface to be reconstructed is implicitly represented as the zero

level set of a signed distance function d. Thereby, no parameterization of the surface is required and complex topologies can be handled easily. In order to define d and thus the surface, all contours are sampled at N equidistant points in total and the points are transformed to world coordinates. These points are assigned a distance of 0. In addition, the planar normal for each point is calculated, too. These normals can be analytically determined from the spline curves. At the intersection [1] of two contours, both planar normals can be extended to 3-D using the non-planar component of the respective other normal. For the N points sampled from the contours, the missing component of the normal is then found by linear interpolation between the respective components of the two closest intersections, as illustrated in Fig. 2(c). The linear interpolation is performed according to the arc length distances along the respective contour. Given the N points in world coordinates and their 3-D normals, $2N$ additional constraints can be defined for the signed distance function d by moving each point one length unit in its positive and negative normal direction and assigning that point a signed distance value of $+1$ or -1, respectively. This sparse signed distance function containing all $3N$ points denoted with $\boldsymbol{p}_i$ is interpolated using radial basis functions according to

$$d(\boldsymbol{x}) = q(\boldsymbol{x}) + \sum_{i=1}^{3N} \varphi(|\boldsymbol{x} - \boldsymbol{p}_i|)\,\lambda_i, \tag{1}$$

where q is a polynomial of degree 1 and "$|.|$" denotes the Euclidean norm. We use the biharmonic kernel $\varphi(t) = t$, which ensures a smooth surface reconstruction [11]. The fitting of polynomial coefficients and the estimation of interpolation coefficients is described in [11]. In order to keep the fitting and evaluation time small, N is chosen in the range $300 < N < 500$. In our experiments, we found this usually sufficient to capture most if not all of the detail the user has specified when drawing the contours. Furthermore, it is not necessary to capture all detail with the initial surface due to the subsequent surface evolution. The interpolation is performed on a grid with spacing h, where h is the minimum spacing of the dataset. Evaluating (1) for the whole grid containing the liver is not necessary and would be too time-consuming. Instead, the surface is traced and the signed distance function is only evaluated at grid nodes belonging to grid cells which are intersected by the surface. In order to generate a rendering of the surface, as shown in Fig. 2(d), each intersected grid cell is polygonized according to the Marching Cubes algorithm [12].

[1] To aid the definition of intersecting contours, the intersection points of all other contours with the current slice are shown. When performing a new delineation, spline control points are then placed such that the curve passes through these intersection points. As this will usually not yield true intersections, two contours are considered to intersect if the distance between their closest points is below a threshold.

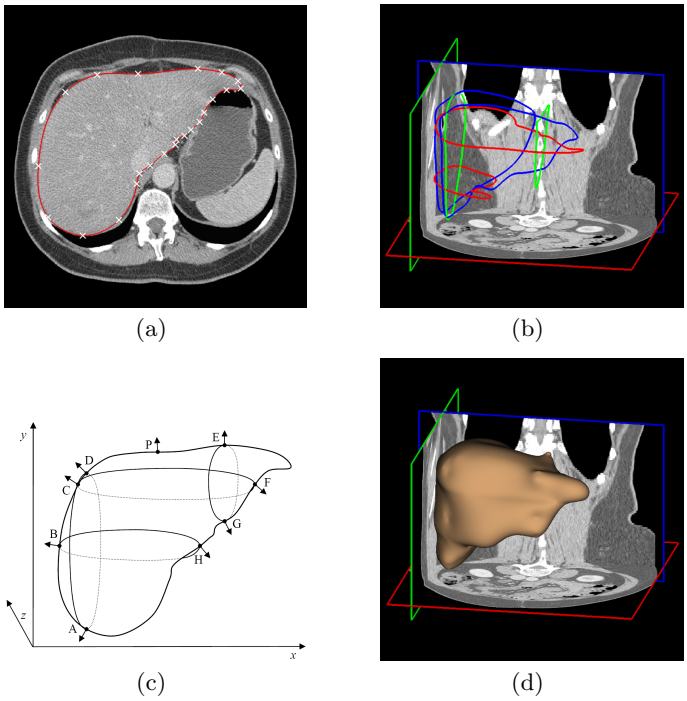

Fig. 2. (a) Manual delineation of a liver cross-section; spline control points are denoted with "×". (b) Six cross-sectional contours are defined, two for each orthogonal view orientation. (c) Visualization of calculated 3-D normals; at the points A – H, the planar normal of the contour defined in the x/y plane is extended to 3-D using the z-components of normals of intersecting contours defined in x/z and y/z planes, respectively; the z-component of the normal at P is determined by linear interpolation between the z-components at D and E according to the arc length distances from D to P and from P to E. (d) Rendering of the interpolated surface.

3 Surface Evolution

The initial surface calculated only with contour information passes through the manual delineations. In distant regions, we found it to be a good approximation of the actual organ shape. In order to improve accuracy, the surface is evolved in a second step using both image and contour information. Evolving the surface solely using image information would forfeit the valuable information of the manual delineations and fail for low-contrast or missing boundaries, as illustrated in Fig. 1(b). As mentioned before, our paradigm is to specify shape information where image content is ambiguous. In other regions, image information is used, freeing the user from having to perform numerous manual segmentations.

The level set evolution takes place using the same grid as the initial surface reconstruction. We decided for edge-based Geodesic Active Contours [7], because we want pathologic structures to be included in the segmentation and the sta-

tistical information required for region-based approaches is often destroyed by such structures. The level set function ϕ that represents the deforming surface through its zero level set is evolved according to

$$\frac{\partial \phi(\boldsymbol{x})}{\partial t} = |\nabla \phi(\boldsymbol{x})| \operatorname{div}\left(g(|\nabla I(\boldsymbol{x})|) \frac{\nabla \phi(\boldsymbol{x})}{|\nabla \phi(\boldsymbol{x})|} \right), \tag{2}$$

where I is the input image or volume, g is a stopping function [7], and "div" denotes the divergence operator. Most level set applications use a constant speed component to drive the deforming surface to object boundaries. With the initial surface calculated in the previous step being a good estimate of the actual organ shape, no such constant speed, which might drive the deforming surface across weak boundaries (see Fig. 1(b)), is necessary here.

In order to incorporate the shape information, a method is required which fits a surface to a set of contours or contour points. As the surface reconstruction will be combined with the level set segmentation, the RBF approach described before cannot be used again. We instead employ the level set surface reconstruction approach proposed in [13], which can be combined straightforwardly with the level set segmentation. While delivering locally smooth surfaces, the level set reconstruction method lacks the higher order global smoothness of the RBF reconstruction in regions with a sparse set of input points, which prohibits using it for determining the initial surface. Now the shape information shall only influence the deforming surface in regions close to predefined contours. The level set surface reconstruction is well suited for that task.

Given a set of points, the level set surface reconstruction finds a surface which is smooth and which minimizes an energy taking the distance of the evolving surface to the points into account [13]. The according level set equation is

$$\frac{\partial \phi(\boldsymbol{x})}{\partial t} = |\nabla \phi(\boldsymbol{x})| \operatorname{div}\left(\delta(\boldsymbol{x}) \frac{\nabla \phi(\boldsymbol{x})}{|\nabla \phi(\boldsymbol{x})|} \right), \tag{3}$$

where δ is the distance function to the input points. In contrast to the surface reconstruction using radial basis functions presented in the previous section, this approach relies only on the unsigned distance function, no normals are required. We calculate δ for (3) using the fast sweeping algorithm [14]. Therefore M input points are sampled in total from all contours. With the fast sweeping algorithm having linear complexity in both the number of input points M and the number of grid points, M can be chosen large, e.g. $M = 10N$, ensuring that the shape constraint captures all detail the user has specified when defining the initial contours.

Combining (2) and (3), the joint image and shape information evolution equation takes the form

$$\frac{\partial \phi}{\partial t} = |\nabla \phi| \operatorname{div}\left((\mu(\delta) g(|\nabla I|) + (1 - \mu(\delta)) \delta) \frac{\nabla \phi}{|\nabla \phi|} \right). \tag{4}$$

The spatial position $\boldsymbol{x}$ is omitted in (4) for the sake of a simpler notation. μ is a function that weights the influence of each component with respect to the

Dataset	Overlap Error		Volume Diff.		Avg. Dist.		RMS Dist.		Max. Dist.		Total
	[%]	Score	[%]	Score	[mm]	Score	[mm]	Score	[mm]	Score	Score
1	10.1	61	10.0	47	1.7	58	2.6	64	20.0	74	61
2	9.7	62	8.7	54	1.5	63	2.6	63	27.3	64	61
3	8.7	66	5.3	72	1.8	55	3.1	57	26.2	65	63
4	13.1	49	13.5	28	2.5	37	4.1	43	25.3	67	45
5	10.9	57	10.1	46	2.1	47	3.6	50	35.1	54	51
6	7.6	70	3.1	84	1.2	70	2.4	67	23.8	69	72
7	9.1	65	8.7	54	1.4	64	2.3	68	16.6	78	66
8	11.1	57	11.4	39	2.0	51	2.7	63	13.7	82	58
9	10.1	61	8.6	54	1.4	65	2.3	69	19.7	74	65
10	10.9	57	8.6	54	1.9	53	3.1	57	18.8	75	59
Average	10.1	60	8.8	53	1.7	56	2.9	60	22.6	70	60

Table 1. Results of the comparison metrics and scores for all ten test cases.

distance from a manually delineated contour. We have chosen a sigmoid function for μ, whose shift and slope control the width and offset of the transition band from pure shape based evolution ($\mu = 0$) to pure image based evolution ($\mu = 1$).

4 Results

The proposed algorithm has been evaluated for ten abdominal CT scans of the liver. The segmentation results were compared to manual expert segmentations and given a score. The scale was set such that a score of 100 points was awarded to a perfect liver segmentation with 100% volume overlap and a score of 75 points was awarded to a segmentation with a volumetric overlap error of 6.4%, a relative absolute volume difference of 4.7%, an average symmetric absolute surface distance of 1.0mm, a symmetric RMS surface distance of 1.8mm, and a maximum symmetric absolute surface distance of 19.0mm. These values reflect deviations of a typical manual segmentation from the perfect reference segmentation. The results are presented in Table 1. Figure 3 shows the segmented liver boundary and the reference boundary for a selection of slices. The initial and final position of the surface is illustrated in figure 4(a), figure 4(b) shows a rendering of the segmented liver shape of dataset No. 6.

Defining the initial contours involves selecting MPR slices and placing spline control points in them. This typically took around 5 min. in total for six to eight manual delineations. Our non-optimized implementation performed the reconstruction of the initial surface in usually less than 2 min., evolving the surface took 2.5 to 5 min. on standard computational hardware.

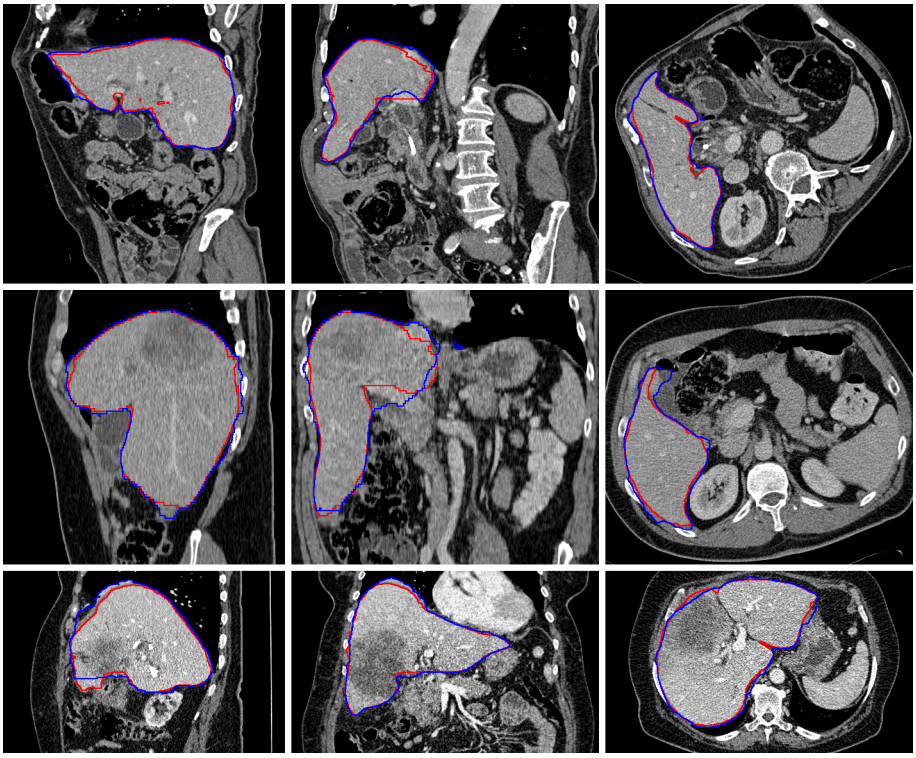

Fig. 3. From left to right, a sagittal, coronal and transversal slice from a relatively easy case (1, top), an average case (4, middle), and a relatively difficult case (3, bottom). The outline of the reference standard segmentation is in red, the outline of the segmentation of the method described in this paper is in blue. Slices are displayed with a window of 400 and a level of 70.

5 Discussion and Conclusion

We have presented a novel two-stage semi-automatic algorithm for the 3-D segmentation of complex organ structures and demonstrated its value for the segmentation of the liver. In the first stage, the user manually delineates cross-sections of the anatomical structure. Given these contours, an initial surface is interpolated using radial basis functions. In the second stage, this surface is automatically evolved under the level set framework using a new combination of both image and shape information.

Combining manual delineation with automatic surface reconstruction and image segmentation has several advantages. With the reconstructed surface providing a good initialization, only a few level set iterations are required until the equilibrium between image- and shape-derived speed components is reached. In addition, a constant speed component, which might drive the deforming sur-

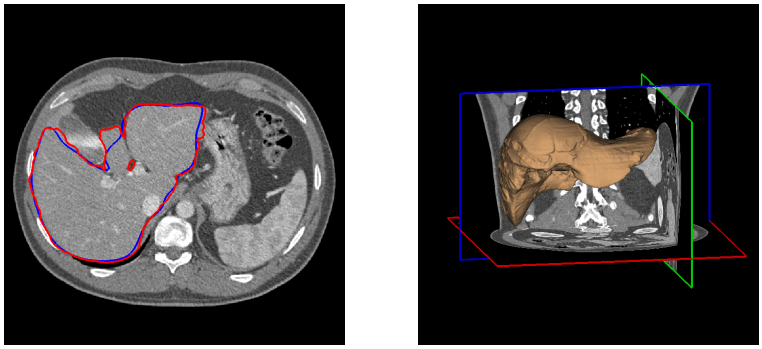

(a) (b)

Fig. 4. (a) Starting at the position marked in blue, the initial surface deforms using both image and shape information to the final position marked in red. (b) Rendering of the segmented liver surface of dataset No. 6.

face across weak boundaries, is superfluous. During the surface evolution, shape information is used in areas close to manually delineated contours. Thereby, ambiguous image content can be resolved by the user. In other areas, image information prevails, thus reducing the required number of manual delineations. Another benefit of our approach is that no underlying model of the shape characteristics and therefore no training phase is required.

The results listed in Table 1 show that the semi-automatic algorithm is able to accurately segment the liver. While it does not reach the score of a manual segmentation, the required amount of user-interaction is significantly smaller, only 7 slices on average were manually delineated.

The main cause for segmentation errors is an initial surface including high-contrast boundaries not belonging to the liver. Such boundaries are for example encountered for ribs, the right kidney, or in areas where organ or muscle tissue is adjacent to fat. During the deformation stage, the surface will usually stick to those spurious boundaries. An accurate initialization is also of high importance for the central part of the liver, which has an extremely complex anatomy due to separating lobes and branching vessels. Otherwise, the deforming surface may fail to recover concave regions or to exclude vessels. This usually leads to an oversegmentation and can be observed especially for the datasets No. 4 and 5. In both cases, the initial surface was reconstructed from six delineations.

The afore-mentioned problems can be solved by specifying additional contours in regions where the initial surface is inaccurate. Even a single additional contour often leads to a drastic improvement. With our non-optimized implementation taking around two minutes for the surface reconstruction, future work will focus on increasing the performance. Having a prompt reconstruction from the specified set of contours would conveniently allow the user to add exactly the required amount of information. Instead of specifying additional contours, the problem of the surface sticking to spurious high-contrast boundaries between

muscle or organ tissue and fat might also be addressed by incorporating intensity information in the deformation stage. With fat having characteristic absorption values in CT images, the surface could be forced to retract from those regions erroneously included in the initialization and to move back to the liver.

References

1. Leventon, M.E., Grimson, W.E.L., Faugeras, O.D.: Statistical shape influence in geodesic active contours. In: CVPR. (2000) 1316–1323
2. Soler, L., Delingette, H., Malandain, G., Montagnat, J., Ayache, N., Koehl, C., Dourthe, O., Malassagne, B., Smith, M., Mutter, D., Marescaux, J.: Fully automatic anatomical, pathological, and functional segmentation from ct scans for hepatic surgery. In Hanson, K.M., ed.: Proc. SPIE Medical Imaging 2000: Image Processing. Volume 3979 of Presented at the Society of Photo-Optical Instrumentation Engineers (SPIE) Conference. (2000) 246–255
3. Heimann, T., Wolf, I., Meinzer, H.P.: Active shape models for a fully automated 3d segmentation of the liver – an evaluation on clinical data. In Larsen, R., Nielsen, M., Sporring, J., eds.: Medical Image Computing and Computer-Assisted Intervention – MICCAI 2006. Volume 4191 of LNCS., Springer (2006) 41–48
4. Schenk, A., Prause, G.P.M., Peitgen, H.O.: Efficient semiautomatic segmentation of 3d objects in medical images. In: MICCAI 2000: Proceedings of the Third International Conference on Medical Image Computing and Computer-Assisted Intervention, Springer-Verlag (2000) 186–195
5. Falcao, A.X., Udupa, J.K., Samarasekera, S., Sharma, S., Hirsch, B.E., de A. Lotufo, R.: User-steered image segmentation paradigms: live wire and live lane. Graph. Models Image Process. **60**(4) (1998) 233–260
6. Grady, L.: Random walks for image segmentation. IEEE Transactions on Pattern Analysis and Machine Intelligence **28**(11) (2006) 1768–1783
7. Caselles, V., Kimmel, R., Sapiro, G.: Geodesic active contours. In: ICCV. (1995) 694–699
8. Sethian, J.A.: Level Set Methods and Fast Marching Methods. second edn. Cambridge University Press (1999)
9. Späth, H.: One Dimensional Spline Interpolation Algorithms. AK Peters (1995)
10. Turk, G., O'Brien, J.F.: Shape transformation using variational implicit functions. In: SIGGRAPH '99: Proceedings of the 26th annual conference on Computer graphics and interactive techniques, New York, NY, USA, ACM Press/Addison-Wesley Publishing Co. (1999) 335–342
11. Carr, J.C., Beatson, R.K., Cherrie, J.B., Mitchell, T.J., Fright, W.R., McCallum, B.C., Evans, T.R.: Reconstruction and representation of 3d objects with radial basis functions. In: SIGGRAPH '01: Proceedings of the 28th annual conference on Computer graphics and interactive techniques. (2001) 67–76
12. Lorensen, W.E., Cline, H.E.: Marching cubes: A high resolution 3d surface construction algorithm. In: SIGGRAPH '87: Proceedings of the 14th annual conference on Computer graphics and interactive techniques. (1987) 163–169
13. Zhao, H.K., Osher, S., Fedkiw, R.: Fast surface reconstruction using the level set method. In: Proceedings of the IEEE Workshop on Variational and Level Set Methods (VLSM'01), Washington, DC, USA, IEEE Computer Society (2001) 194
14. Zhao, H.K.: A fast sweeping method for eikonal equations. Mathematics of Computation **74** (2005) 603–627